Correlations between Reduction Degree and Catalytic Properties of WO_x Nanoparticles

Febrigia Ghana Rinaldi[1], Osi Arutanti[2], Aditya Farhan Arif[1], Tomoyuki Hirano[1], Takashi Ogi[1], Kikuo Okuyama [1]*

[1]Department of Chemical Engineering, Graduate School of Engineering, Hiroshima University, 1-4-1 Kagamiyama, Higashi Hiroshima 739-8527, Japan

[2]Research Center for Nanosciences and Nanotechnology (RCNN), Institut Teknologi Bandung, Jl. Ganesha 10, Bandung 40132, Indonesia

*Corresponding Author: E-mail: ogit@hiroshima-u.ac.jp; Tel.: +81-82-424-3675

S1. Morphology of the WO_x Nanoparticles Reduced at 400 - 475 °C

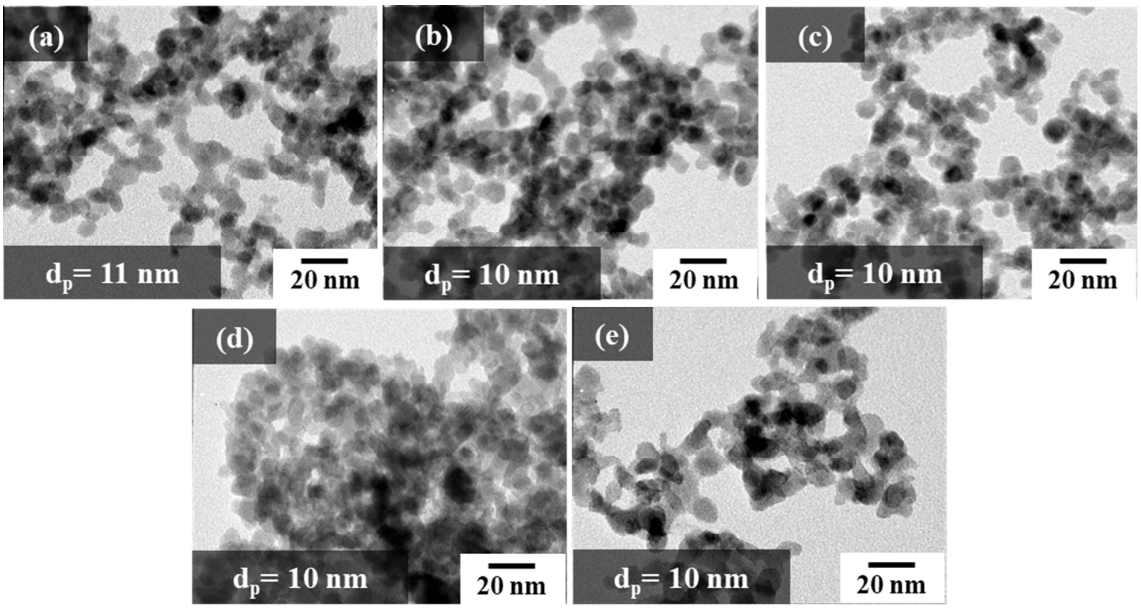

Figure S1. TEM images of the as-synthesized WO_x NPs reduced at (a) 400, (b) 415, (c) 425, (d) 450, (e) 475 °C

S2. Raman Spectroscopy Analysis

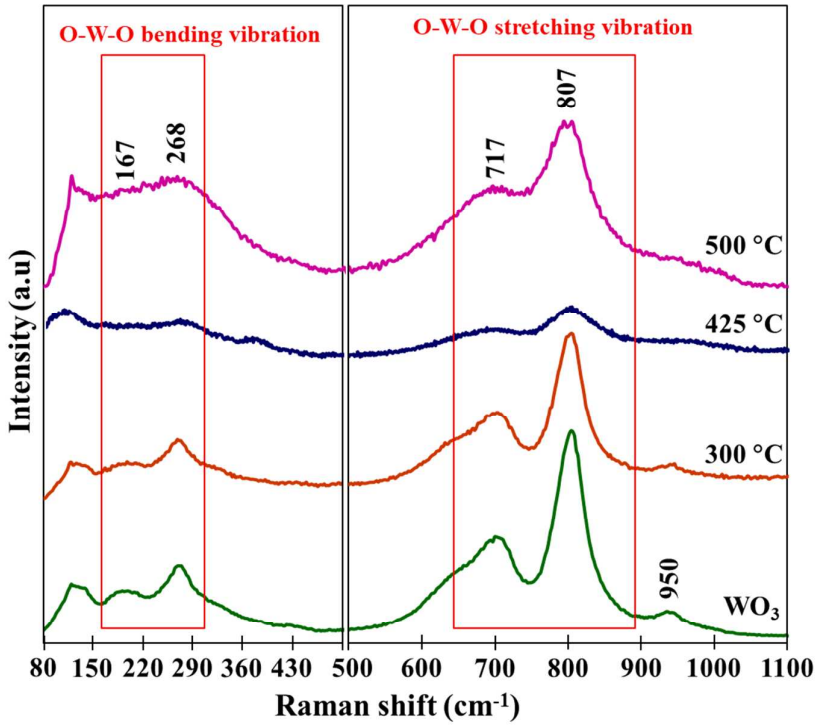

Figure S2. Raman spectra of the WO_3 NPs and WO_x NPs reduced at different temperatures.

The left side shows the short wavelength region from 80 to 500 cm^{-1} that corresponds to the region for the bending vibration of O-W-O bonding. The right side shows the long wavelength region from 500 to 1100 cm^{-1} that corresponds to the region for the stretching vibration of O-W-O bonding. In both sections, the Raman spectrum of the WO_3 NPs shows a sharp line with several strong, well-defined peaks of the monoclinic crystalline phase at 167, 268, 717, and 807 cm^{-1}. This indicated high crystallinity of the WO_3 crystal structure.

In the left section, the peak at 268 cm^{-1} was assigned to the W^{6+} state.[1] When the reduction temperature was 300 °C, the Raman spectrum of the obtained WO_x NPs showed similar peaks with those in the spectrum of the WO_3 NPs, but with lower peak intensity, especially for the peak at 167 cm^{-1}. The weakening of the O-W-O bonding vibration in the spectrum of the WO_x (300 °C) NPs indicated the presence of oxygen vacancies, which affected the angle between the W and O atoms.[1] In the spectrum of WO_x (425 °C) NPs, the two peaks in the left section were hardly observed. This indicated that the number of oxygen vacancies within the crystal structure was higher than in WO_x NPs synthesized at lower temperatures. A similar result was obtained when the reduction temperature was further increased to 500 °C.

In the right section, the W-O stretching vibration was influenced by the change in bond length. **Figure S2** shows that the Raman spectrum of the WO_3 NPs had the strongest peaks of O-W-O stretching vibrations among the samples. Similar spectra were obtained for WO_x NPs reduced at 300 and 500 °C. These results were consistent with the XRD patterns in **Figure S2**, in which WO_x (300 °C) NPs and WO_x (500 °C) NPs both mainly consisted of the WO_3 monoclinic structure. The Raman spectrum of the WO_x (425 °C) NPs had the weakest peak intensities for the O-W-O stretching vibration. This indicated that the presence of oxygen vacancies resulted in a change in bond length between the W and O atoms. The small peak at

950 cm^{-1} was assigned to the presence of W=O groups.[1] This small peak weakened and disappeared when the reduction temperature was increased to 425 °C.

S3. XPS Measurement Results

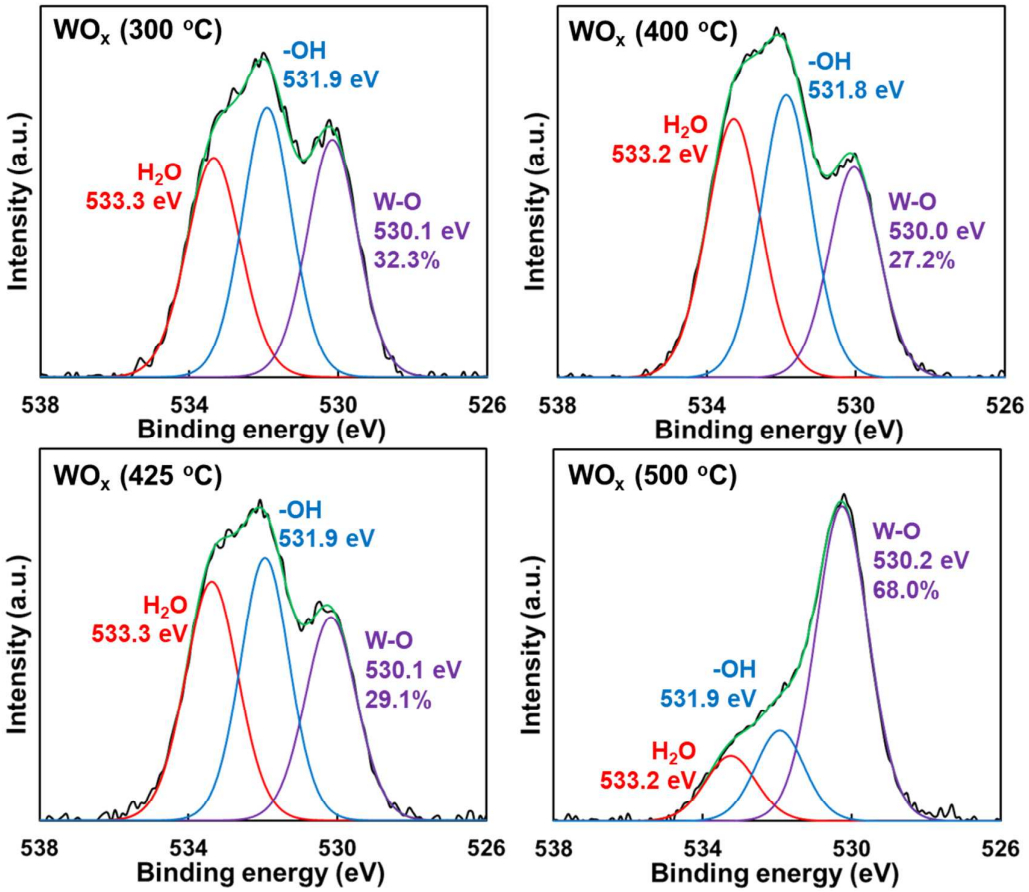

Figure S3. XPS results at binding energies around O 1s orbital for WO_x nanoparticles reduced at 300, 400, 425, and 500 °C. All fittings were done with reduced chi-squared values below 50.

Each measurement around the O 1s orbital shows three observable peaks at binding energy of 530, 531.9, and 533.3 eV that correspond to W-O bonding, hydroxyl group (-OH), and water molecule, respectively. [2-3]

S4. Band Gap Value Analysis

The band gap value for every sample was obtained by using a common method called Tauc plot. [4] This plot is based on an equation derived by Tauc, Davis, and Mott [5] as follows:

$$(h\nu\alpha)^{1/n} = A(h\nu - E_g) \quad \textbf{(S1)}$$

where:

h = Planck's constant ($6.626 \cdot 10^{-34}$ kgm^2s^{-1})

ν = Frequency of vibration

α = Absorption coefficient

A = Proportional constant

E_g = Band gap energy

The value of n depends on the nature of the transition for electrons moving from the valence band to the conduction band. It is equal to ½ and 2 for direct and indirect allowed transition, whereas it is 3/2 and 3 for direct and indirect forbidden transition, respectively.

The following calculation is an example using the results of the diffuse reflectance measurement for the WO_3 nanoparticles. From the obtained diffuse reflectance spectrum, as shown in **Figure S4**, a function of reflectance ($F(R)$) is calculated based on the following Kubelka-Munk equation [6]:

$$F(R) = \frac{(1-R)^2}{2R} \quad \textbf{(S2)}$$

This $F(R)$ constant can be substituted to **Equation (S1)** replacing the α coefficient so that it can be written as:

$$(h\nu F(R))^{1/n} = A(h\nu - E_g) \quad \textbf{(S3)}$$

For tungsten oxide, the nature of electron movement from the valence band to the conduction band is indirect allowed transition. Therefore, a value of 2 is used for the n constant. The value of $h\nu$ is calculated based on the following equation:

$$h\nu = \frac{1239.7}{\lambda} \quad \textbf{(S4)}$$

where λ is the irradiated light wavelength used in the diffuse reflectance measurement, as shown in **Figure S4**.

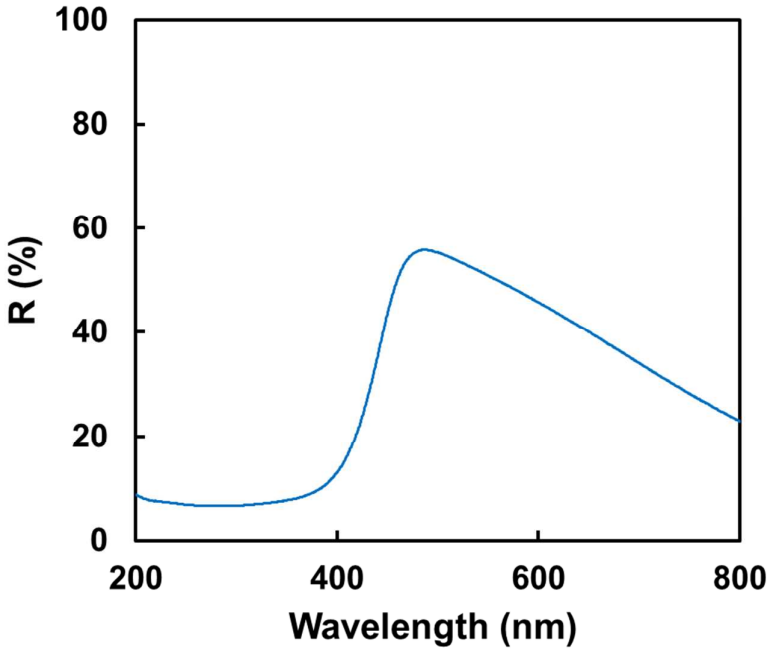

Figure S4. Diffuse reflectance spectrum for WO_3 nanoparticles

Based on the **Equation (S2)**, **(S3)**, and **(S4)**, the value of $(h\nu F(R))^{1/2}$ is plotted against $h\nu$ the result is shown in **Figure S5**. From this Tauc plot, a tangent line is drawn at the inflection point of the curve, and the value of the band gap energy (E_g) can be obtained from the intersection point between the x axis and the tangent line.

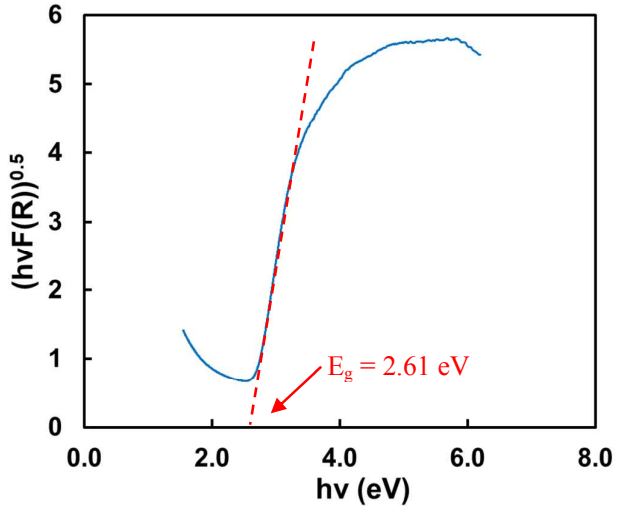

Figure S5. Tauc plot obtained for the WO_3 nanoparticles using the Kubelka-Munk relation

The summary of diffuse reflectance spectra and Tauc plots for the WO_3 and WO_x NPs is shown in **Figure S6.** When the WO_3 NPs were reduced at 300 °C, the amount of oxygen vacancies was low. However, their absorption was increased across the entire measurement window compared with the WO_3 NPs, as shown in **Figure S6(a)**. When the WO_3 NPs were reduced at 400–500 °C, a significant improvement in the absorption of the WO_x NPs at long wavelengths was observed in **Figure S6(a)** and **S6(b)**. This indicated the dominance of absorption by the reduced W ions over W^{6+} within the NP structure. The free electrons within the NPs allowed them to absorb in the long wavelength region.

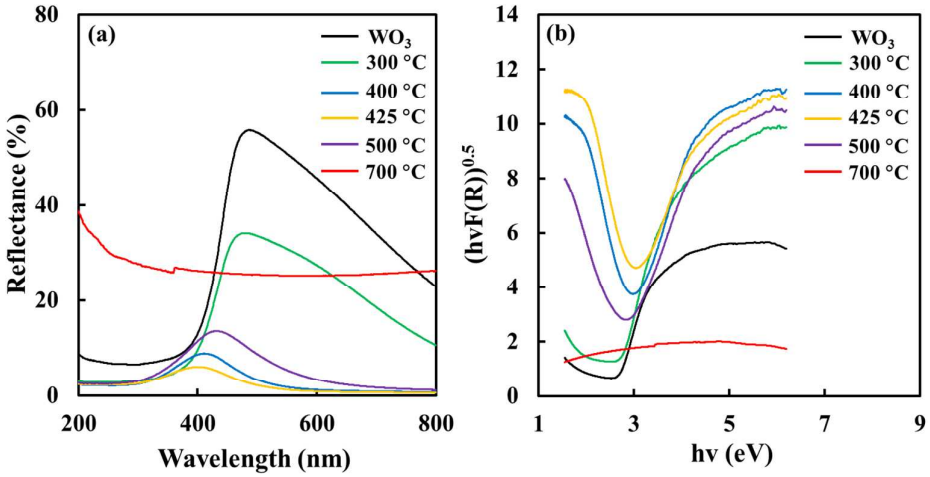

Figure S6. (a) Diffuse reflectance spectra and (b) Tauc plots for the WO_3 NPs and WO_x NPs reduced at different temperatures.

From the calculated band gap values, valence and conduction band energies were estimated for WO_3 [7], WO_x (425 °C), and WO_x (500 °C) NPs, which can be seen in **Figure S7**. From **Figure S7**, it can be concluded that the electrons in the conductions bands of each sample are able to reduce O_2 to H_2O_2, which then captures electrons to generate OH•. Furthermore, the hole in the valence bands of each sample are able to oxidize OH^- and H_2O to OH•. The generated hydroxyl radicals then degrade the RhB molecules following the advanced oxidation processes (AOPs). A proposed schematic illustration of RhB degradation mechanism over the WO_x NPs is shown in **Figure S8**.

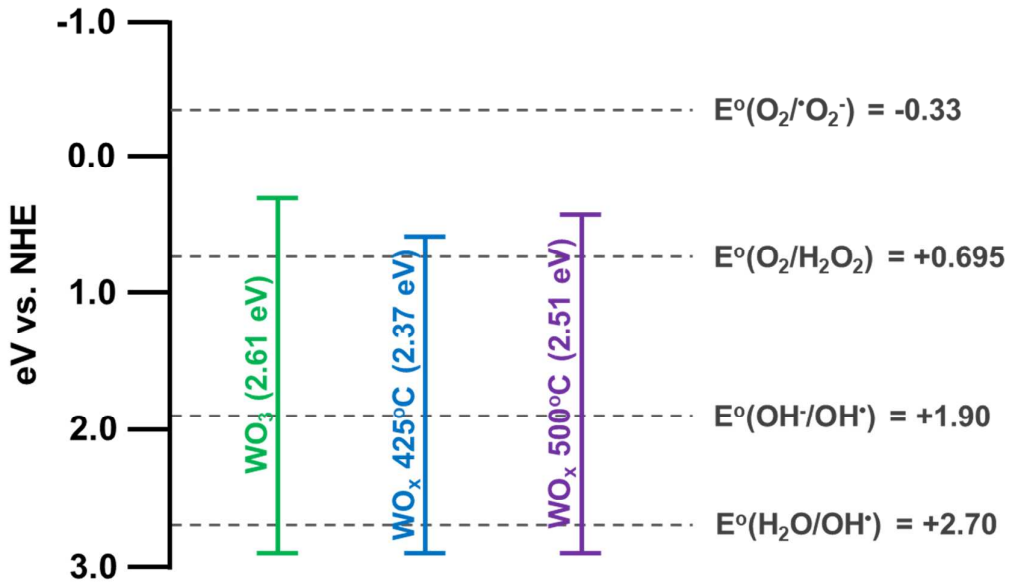

Figure S7. Band energies of WO_3, WO_x (425 °C), and WO_x (500 °C). The values on the right side represent the redox potentials of several reactions that commonly contribute in degradation of rhodamine B.

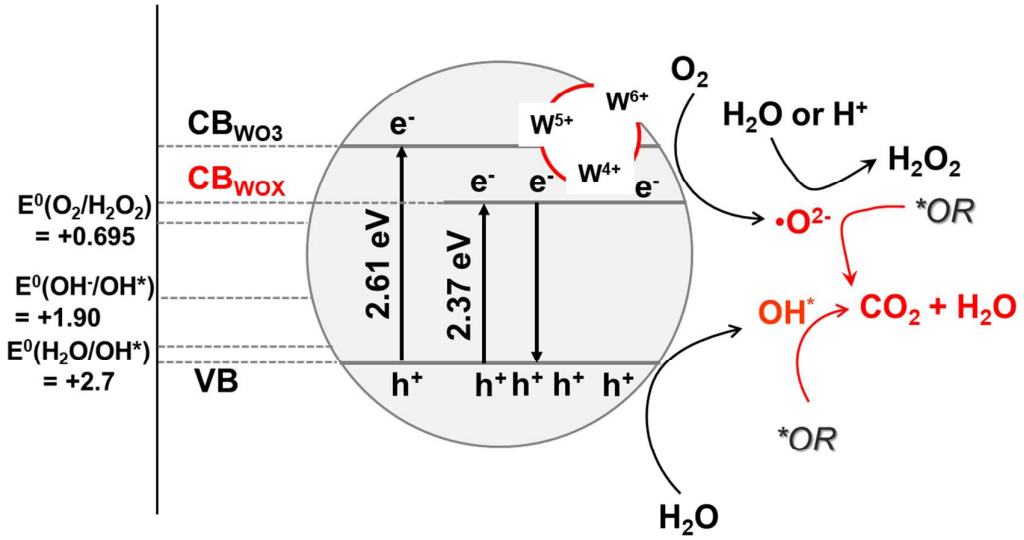

Figure S8. Proposed schematic illustration of RhB degradation mechanism on WO_x surface

References

1. Tian, Y.; Cong, S.; Su, W.; Chen, H.; Li, Q.; Geng, F.; Zhao, Z., Synergy of $W_{18}O_{49}$ and polyaniline for smart supercapacitor electrode integrated with energy level indicating functionality. *Nano letters* **2014,** *14* (4), 2150-2156.
2. Li, J.; Liu, Y.; Zhu, Z.; Zhang, G.; Zou, T.; Zou, Z.; Zhang, S.; Zeng, D.; Xie, C., A full-sunlight-driven photocatalyst with super long-persistent energy storage ability. *Sci Rep* **2013,** *3*, 2409.
3. Ji, R.; Zheng, D.; Zhou, C.; Cheng, J.; Yu, J.; Li, L., Low-temperature preparation of tungsten oxide anode buffer layer via ultrasonic spray pyrolysis method for large-area organic solar cells. *Materials (Basel)* **2017,** *10* (7).
4. Tauc, J.; Grigorovici, R.; Vancu, A., Optical properties and electronic structure of amorphous germanium. *physica status solidi (b)* **1966,** *15* (2), 627-637.
5. Davis, E.; Mott, N., Conduction in non-crystalline systems V. Conductivity, optical absorption and photoconductivity in amorphous semiconductors. *Philosophical Magazine* **1970,** *22* (179), 0903-0922.
6. Kubelka, V. P., Ein beintrag zur optik der farbanstriche. *Zeits. fur techn. Physik* **1931,** *12*, 593-601.
7. Highfield, J., Advances and recent trends in heterogeneous photo(electro)-catalysis for solar fuels and chemicals. *Molecules* **2015,** *20* (4), 6739-93.